Noise-assisted transmission of binary information: Theory and experiment

Sylvain Barbay,[1] Giovanni Giacomelli,[1,2,*] and Francesco Marin[2,3]
[1]*Istituto Nazionale di Ottica Applicata, Largo E. Fermi 6, 50125 Firenze, Italy*
[2]*Istituto Nazionale di Fisica della Materia, unità di Firenze, Firenze, Italy*
[3]*Dipartimento di Fisica, Università di Firenze, and Laboratorio Europeo di Spettroscopia Nonlineare, Largo E. Fermi 2, 50125 Firenze, Italy*

(Received 20 October 2000; published 23 April 2001)

We study the response of a bistable vertical cavity surface emitting laser to an aperiodic binary signal, by adding a variable amount of noise. The resulting behavior is an example of aperiodic stochastic resonance, and in this work we give a detailed comparison between analytical and numerical results and accurate experimental measurements. We characterize the phenomenon by using different appropriate indicators, which also allow us to quantify the binary information transmission. We show that the quality of the transmission is enhanced by a suitable amount of noise, and we give a physical picture of the phenomenon.

DOI: 10.1103/PhysRevE.63.051110 PACS number(s): 05.40.Ca, 42.65.Pc, 42.55.Sa, 02.50.Ey

I. INTRODUCTION

The activity in the field of stochastic processes, and in particular of noise-induced ordering, has intensified during the last years. This subject is now recognized as extremely important in a large variety of fields, ranging from biology and geology, to information theory and physics. An important example of these phenomena is represented by stochastic resonance (SR). SR is a specific response of bistable systems to a sinusoidal modulation in the presence of noise. An improvement of the quality of the output signal is observed as the amount of noise is increased, up to an optimal (resonant) value. SR was introduced in 1981 [1,2] to explain the periodicity of the continental ice volume in the quaternary era, and it has been the object of extensive investigations, mainly since the experimental evidence in a bistable ring laser [3]. SR has been studied in detail with analogic simulations and with analytical and numerical investigations [4]. Recently, the observation of SR in the dynamical behavior of a vertical cavity surface emitting laser (VCSEL) [5] has provided experimental results of the same quality of model simulations, allowing one to directly verify many of the predictions of the theory [6].

SR is often considered as an intriguing mechanism to improve the quality of signal transmission in nonlinear systems. However, while investigations of SR have provided important insights into the physics of noise-induced resonance, the generalization from a sinusoidal shaped to an arbitrarlly shaped large input signal is not straightforward. This is simply suggested by the fact that the matching condition between the input signal frequency and the Kramers rate, typical of SR, cannot be obviously applied to nonperiodic signals.

The analysis of the response of noisy, bistable systems to small, *aperiodic* signals was recently addressed. In 1994 Neiman and Schimansky-Geier [7] studied the transmission through a noisy, bistable system of a particular signal, namely, harmonic noise. The term aperiodic stochastic resonance (ASR) was coined in Ref. [8], referring to the amplification of sub-threshold, random signals in the Fitz-Hugh-Nagumo model of an excitable system. The system undergoes a resonant regime which can be shown by evaluating the cross-correlation of the output vs the input signal. The theoretical and numerical analysis was extended in Ref. [9] to several kind of systems. Further theoretical and numerical studies of the response of a noisy system to binary, random input signal were reported in Refs. [11] and [10].

This large amount of modeling effort was motivated by the study of the role of noise in the perception mechanism. Several observations of related phenomena in biological systems were recently reported [12]. These works are of great value due to the clear signature of the phenomena presented. However, the quality of the measurements cannot be sufficient for checking the full predictions of the models.

The situation is different in Ref. [13], where we experimentally investigated the response of a bistable, optical system to a random, binary (telegraph) signal, changing the amount of applied external noise. In that preliminary work, we showed experimental evidence of ASR, with excellent reproducibility, and a control of the parameters, which made the work qualitatively different from previous observations, to our knowledge.

The particular kind of signal considered is not only very useful for a basic understanding of the physical mechanism, but is also of particular interest in digital communications. We discussed this aspect in a previous paper [14] devoted to the noise-enhanced binary signal transmission in optical communications.

In this paper, we summarize and detail the experimental results first presented in Ref. [13], and describe the theoretical models which allow for an excellent reproduction of the experimental findings. We derive both analytical and numerical results, yielding a clear physical picture of the noise-induced dynamics.

Besides the dynamical approach, a different point of view in our case is particularly interesting, i.e., the study of the

*Email address: gianni@ino.it

flow of information through a bistable system with a variable input noise. For this purpose, we introduce some specific indicators of the quality of the transmission. In this paper, we present a basic analysis of the phenomenon, studying the single-bit transmission statistics. This approach allows for a clear understanding of the physical processes underlying the observed behavior, and for a simple analytical description.

The paper is organized as follows. In Sec. II we summarize the experimental observations. In Sec. III we introduce and discuss the models, both with analytical and numerical techniques, whose previsions are compared with the experimental results in Sec. IV. In Sec. V we draw our concluding remarks.

II. EXPERIMENTAL RESULTS

Preliminary reports of the experimental observations were given in Refs. [13,14]. The physical system is composed of a VCSEL followed by a polarizer and a detection system (see Ref. [6] for a detailed description of the setup). By sweeping the pump current, the laser can emit in different polarization and transverse profile configurations. The transition between two states is generally characterized by a bistable current region, where noise-induced jumps occur between the two states. The laser dynamics can be reconducted in this case to a van't Hoff–Arrhenius [15,16] process, with average permanence times usually given by a Kramers law, i.e., an exponential function of the noise intensity [17]. By introducing additional noise into the pump current, the statistics of the jumps can thus be changed. The polarization fluctuations are transformed into light intensity variations by the polarizer, and detected by means of a photodiode whose signal is acquired by a digital scope. The signals from a variable intensity, white-noise generator (10-MHz bandwidth) and a pseudorandom binary sequence generator are summed and coupled into the laser input current. The binary sequence is a 16 000-bit word with a bit duration of $T_b = 4\ \mu s$. Its amplitude is 0.27 mA (peak to peak), smaller than the width of the bistable region (0.49 mA). As a consequence, the current steps are not large enough to induce a laser state jump without the aid of the noise.

An example of the signal detected by the photodiode, for different values of the input noise strength, is shown in Fig. 1. For low noise [Fig. 1(a)] the laser mainly remains in its initial state, even if a small amplitude modulation is visible. Increasing the noise, some jumps occur [Fig. 1(b)], and, for an input noise around 400 mV_{rms}, the output follows the input signal very well [Fig. 1(c)]. Finally, for larger noise strengths, the laser dynamics is determined by the noise more than by the input string, with a strong decorrelation between input and output [Figs. 1(d) and 1(e)].

To quantify the observed behavior, we evaluate the cross-correlation between the input and output signals. For each value of the noise we plot the maximum of the normalized correlation

$$C_{IO} = \max_{\tau}\{\overline{[x_{in}(t)-\overline{x_{in}}][x_{out}(t+\tau)-\overline{x_{out}}]}\}, \qquad (1)$$

where the overline denotes the time average, and the variables x_{in} and x_{out} are rescaled with respect to half the difference between the two stable states. The result is shown in Fig. 2. A well defined peak is present at $D \simeq 350\ mV_{rms}$, indicating the optimal reproduction of the input signal. For each value of the noise the cross-correlation has a maximum for a nonzero time lag τ_{max} between input and output. However, we point out that the experimental values of C_{IO} are not significantly changed if a zero time lag is chosen, instead of τ_{max}. For the sake of simplicity, in Sec. III we will present a theoretical analysis, neglecting the time lag. A detailed study of the time lag, i.e., of the synchronization between input and output signals, will be reported elsewhere.

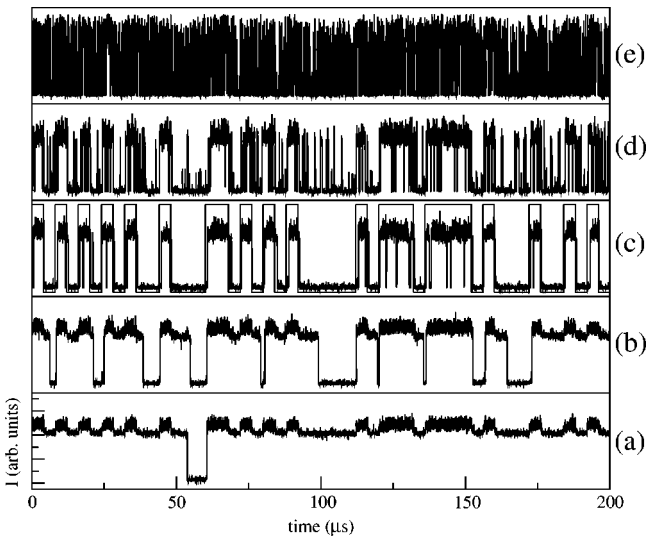

FIG. 1. Polarized laser intensity I for different input noise intensities, with a 50-MHz acquisition bandwidth. (a) 100, (b) 200, (c) 400, (d) 600, and (e) 1200 mV_{rms}. In (c) the input pattern is shown (with an arbitrary vertical scale). A sequence of 50 bits (bit duration 4 μs) is displayed.

As the input signal consists of a binary sequence, it is interesting to study how the associated information is transmitted at the output. We start by defining a procedure to

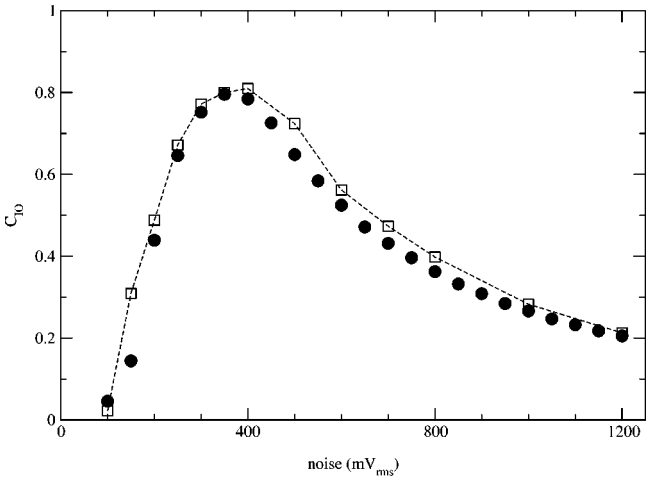

FIG. 2. Normalized cross-correlation between the input and output signals. Dots: experimental data. Squares: analytical results of Eq. (14) using the experimental Kramers times. The dashed line is a guide for the eye.

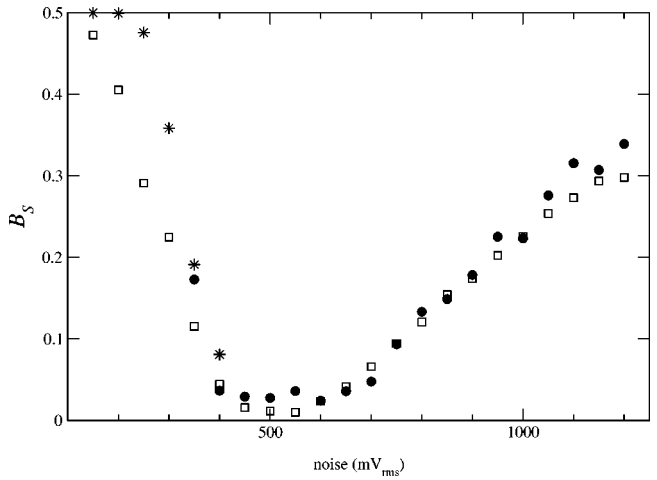

FIG. 3. Bit error rate evaluated by sampling the output signal at the end of the input bit, vs input noise. Squares: experimental results. Circles: analytical results from Eq. (10) using the measured Kramers times. Stars: results using extrapolated Kramers times.

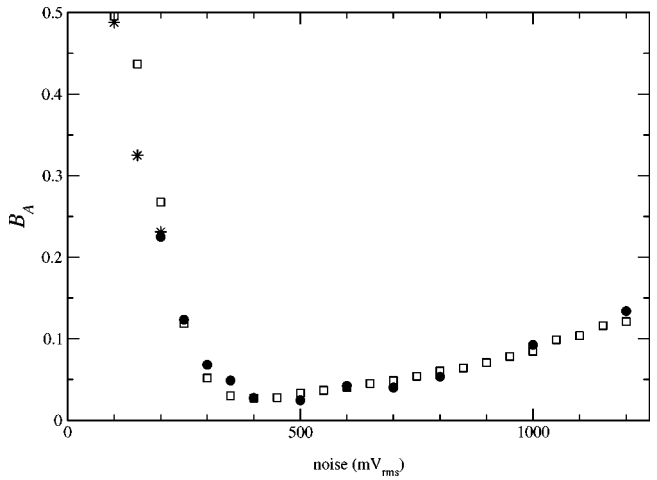

FIG. 4. Bit error rate evaluated by averaging the output signal over the input bit length versus input noise. Squares: experimental results. Circles: analytical resuls from Eqs. (17) and (19) using the measured Kramers times. Stars: results using extrapolated Kramers times.

associate a binary value (0 or 1) to the output signal for each of the time intervals corresponding to the input bits (we assume that the bit length T_b is known).

We use two different methods: the output bit is defined by comparing, with a threshold, either the signal sampled once in the bit or the signal averaged over the bit duration. The threshold value is chosen as the average of the output signal of a sufficiently large number of bits.

Concerning the former procedure, sampling the output signal at the very beginning of the bit gives a result which is strongly reminiscent of the previous bit state. It is clear that the best result is obtained by sampling the signal as late as possible, when the probability distribution of the output state has relaxed to the distribution imposed by the input bit. We therefore take the sample at the end of the bit.

The synchronization between the calculated output string and the input is obtained by shifting the starting point for the averaging process in order to maximize the correlation between input and output strings. This procedure is repeated for each value of the input noise.

The indicator chosen to quantify the transmission quality is the bit error rate (BER) B, defined as the percentage of the wrong transmitted bits. The BER is commonly used in communications, as it represents the simplest way to evaluate the efficiency of a binary data channel. According to the two methods used to assign the output bit value, in the following we will use the notation B_S for the first method and B_A for the second one.

In Fig. 3 we report the experimental measurements of B_S as functions of the input noise D. A clear minimum is found for a well defined value of D. A similar behavior is obtained by measuring B_A (Fig. 4). In this case, a slower increase of the indicator is observed after the minimum.

In the next sections we will compare the experimental findings with the predictions of theoretical models. For this purpose, we will use some experimentally determined parameters in the theoretical expressions. In particular, we measured the average time period spent by the system in the two output levels between two successive jumps. This average time is measured for both output states, and for the two values of the input signal as a function of the noise. If 0 and 1 are the values of the input bit and if we call $-$ and $+$ the corresponding output states, we can define $T_{\pm}^{0,1}$ as the mean time spent in the state $\pm$, respectively, during a given input bit 0 or 1. The measurements were performed by keeping the input level for a long time, i.e., we measured the stationary mean times.

The results are reported in Fig. 5. The measurements are carried out for high enough noise, in order to have sufficient statistics in a reasonable time. The measured mean times, as functions of the inverse of the noise, are well fitted by an exponential function, according to the Kramers law [17], allowing us to extrapolate the results for low noise.

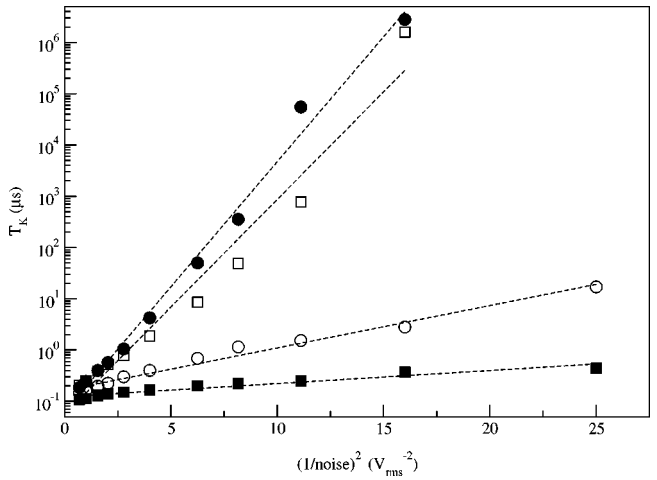

FIG. 5. Experimental Kramers times vs noise: T_-^1 (empty circles), T_-^0 (full circles), T_+^1 (empty squares), and T_+^0 (full squares). The dashed lines are the fit with an Arrhenius law for low noise extrapolation of the times.

III. MODELS

The most widely used model for the VCSEL is the so-called spin-flip model [18]. It has been reduced using adiabatic approximations by Willemsen *et al.* [19], who indeed obtained a local description of the polarization switchings in terms of the two well potentials. A different kind of reduction was described in Ref. [20], where the authors again obtained a local model with a bistable potential. A discussion of the validity of such reductions is beyond the scope of this paper. However, as reported in Refs. [6,21], the dynamics of the laser system can be locally well described by an overdamped Langevin model with a two-well potential.

In Ref. [21] we also showed that a phenomenological potential, obtained from the experimental histograms of the polarized laser intensity, leads to an extremely good prediction of the residence time distributions. However, a simple quartic potential is sufficient to reproduce the features described here. The model considered is based on the Langevin equation

$$\dot{x} = -\frac{\partial V(x,t)}{\partial x} + \xi(t), \tag{2}$$

where $V(x,t) = x^4 - 2x^2 + \mu(t)$; ξ is a white, Gaussian noise term such that $\langle \xi(t)\xi(t') \rangle = 2D \times \delta(t-t')$; $\mu(t)$ is the input signal, i.e., a random binary sequence switching between $-A$ (level 0) and A (level 1) every T_b. The variable x represents the polarized laser intensity.

We integrate Eq. (2) with a second order, stochastic Runge-Kutta algorithm [22]. The integration step is 0.05, the bit height is $A = 0.2$, and the bit length is $T_b = 100$. The solution is sampled with the same rate as the experimental signal, for a better comparison. The results of the simulations are used to verify the analytical expressions found in Secs. III A and III B. This comparison is performed for a symmetric potential, while the analytical calculations are given in a more general, asymmetric case, and directly compared with the experimental results in Sec. IV.

For each value of the input signal, the time evolution of Eq. (2) is characterized by fast jumps between the two stable states $x_\pm$ of the potential $V(x)$. As the switching time is much smaller than the permanence time within the potential wells, a simple description of the dynamics can be carried out in the framework of a two-level model. We introduce the states $\{+,-\}$, corresponding to the system being close to $x_\pm$. We can now use four transition rates $W_\pm^{0,1}$ for the two input levels $\{0,1\}$. The notation is summarized in Fig. 6. We thus assume that the distributions of the residence times are exponential, according to the Arrhenius–van't Hoff law [15,16], as we have experimentally verified,

$$P_\pm^{0,1}(T) = \frac{1}{T_\pm^{0,1}} \exp\left(-\frac{T}{T_\pm^{0,1}} \right), \tag{3}$$

where $T_\pm^{0,1}$ (Kramers times) are the mean time of residence in the state $\pm$ during a given input and $T_\pm^{0,1} = 1/W_\pm^{0,1}$ (see Fig. 6). The underlying assumption is to neglect the intrawell motion.

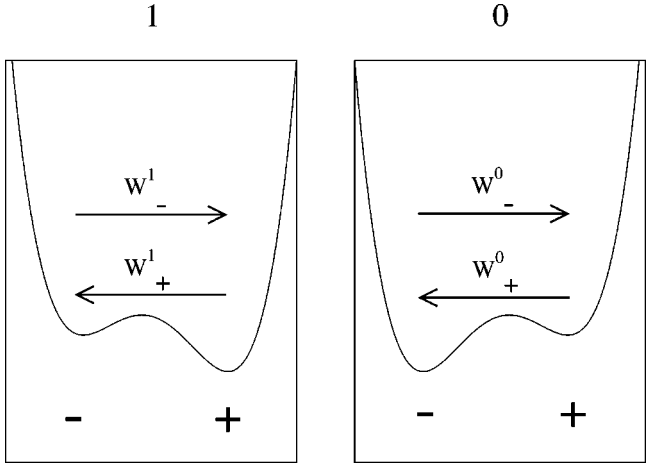

FIG. 6. Definition of the rates for the model.

In the following we consider two simple approaches, which offer a clear picture of the physical processes involved and allow for analytical calculations. In particular, we study the master equations of the two-level model, obtaining an explicit evaluation of B_S and C_{IO}, and we introduce a method to derive the residence time probability distributions within a bit, which in turn are used to evaluate B_A.

A. Master equation approach

We define $n_\pm^{0,1}(t)$ as the two probabilities of being in the states $\{+,-\}$ when the input is 0,1 at the time t after the beginning of the input bit. $n_\pm^{0,1}(t)$ can be calculated using the master equations

$$\begin{aligned} \partial_t n_+^{0,1}(t) &= -W_+^{0,1} n_+^{0,1}(t) + W_-^{0,1} n_-^{0,1}(t), \\ \partial_t n_-^{0,1}(t) &= W_+^{0,1} n_+^{0,1}(t) - W_-^{0,1} n_-^{0,1}(t), \end{aligned} \tag{4}$$

with $n_+^{0,1} + n_-^{0,1} = 1$.

Equations (4) are solved, yielding

$$n_\pm^{0,1}(t) = n_\pm(0) e^{-t\beta_{0,1}} + \alpha_\pm^{0,1}(1 - e^{-t\beta_{0,1}}), \tag{5}$$

where we have introduced $\beta_{0,1} = W_+^{0,1} + W_-^{0,1}$ and $\alpha_\pm^{0,1} = W_\mp^{0,1}/\beta_{0,1}$. We remark that $n_\pm(0)$ does not depend on the actual input bit, but on the previous history.

Due to the random nature of the input signal, the probability for each input bit is equal to 1/2. As a consequence, the initial probabilities are given by

$$n_\pm(0) = \tfrac{1}{2}[n_\pm^1(T_b) + n_\pm^0(T_b)]. \tag{6}$$

Equations (5) and (6) give, as solutions,

$$\begin{aligned} n_\pm^{0,1}(t) = {} & \frac{\alpha_\pm^{0,1}(1 - e^{-T_b\beta_{0,1}}) + \alpha_\pm^{1,0}(1 - e^{-T_b\beta_{1,0}})}{2 - (e^{-T_b\beta_0} + e^{-T_b\beta_1})} e^{-t\beta_{0,1}} \\ & + \alpha_\pm^{0,1}(1 - e^{-t\beta_{0,1}}) \end{aligned} \tag{7}$$

and, at time T_b,

$$n_{\pm}^{0,1}(T_b)=\frac{\alpha_{\pm}^{0,1}(1-e^{-T_b\beta_{0,1}})\left(1-\frac{1}{2}e^{-T_b\beta_{1,0}}\right)+\frac{1}{2}\alpha_{\pm}^{1,0}(1-e^{-T_b\beta_{1,0}})e^{-T_b\beta_{0,1}}}{1-(e^{-T_b\beta_0}+e^{-T_b\beta_1})/2}. \tag{8}$$

The indicator B_S is given by

$$B_S=\tfrac{1}{2}[n_{-}^{1}(T_b)+n_{+}^{0}(T_b)]. \tag{9}$$

Inserting Eq. (8) into Eq. (9), we obtain

$$B_S=\frac{1}{2}\left(1-\frac{(\alpha_{+}^{1}-\alpha_{+}^{0})[1-(e^{-T_b\beta_0}+e^{-T_b\beta_1})+e^{-T_b(\beta_0+\beta_1)}]}{1-(e^{-T_b\beta_0}+e^{-T_b\beta_1})/2}\right). \tag{10}$$

In the symmetric case ($W_{-}^{0}=W_{+}^{1}=1/T_l$ and $W_{+}^{0}=W_{-}^{1}=1/T_s$), we obtain

$$B_S=\frac{1}{2}\left[1-(1-e^{-(1/T_l+1/T_s)T_b})\frac{T_l-T_s}{T_l+T_s}\right]. \tag{11}$$

For a comparison of Eq. (11) with the result of the numerical simulation, we can derive $T_{l,s}$ from the potential $V(x)$, following Kramers [17]. A simplified expression, valid for small A, is

$$T_{l,s}=\frac{\pi}{2\sqrt{2}}\exp\left(\frac{\Delta V\pm A}{D}\right), \tag{12}$$

where the ''+'' refers to T_l, and vice versa, and ΔV is the potential barrier height in the absence of modulation. A more accurate expression takes into account the real shape of the potential with the input signal, and reads [24]

$$T_{\pm}^{0,1}=\frac{2\pi}{\sqrt{V''(x_{\pm})|V''(x_0)|}}\exp\left(\frac{V(x_0)-V(x_{\pm})}{D}\right), \tag{13}$$

x_0 being the unstable point of the potential, which is given for the appropriate value of the input bit.

In Fig. 7 we report a comparison between the integration of the Langevin equation (2) (circles) and the value obtained from Eq. (11), using Eqs. (12) (dashed line) and (13) (dot-dashed line). In spite of the small value of $A=0.2$, the latter expression yields a better agreement at high noise. Such an agreement also confirms that the discrete two-level approximation used for the analytical results is valid.

The correlation C_{IO} can be evaluated by integrating over the bit interval the difference between the probabilities to be in the right and wrong states:

$$C_{IO}=\frac{1}{2T_b}\int_0^{T_b}[(n_{+}^{1}-n_{-}^{1})+(n_{-}^{0}-n_{+}^{0})]dt. \tag{14}$$

In the symmetric case we obtain

$$C_{IO}=\frac{T_l-T_s}{T_l+T_s}\times\left[1-\left(\frac{1-e^{-[(1/T_l)+(1/T_s)]T_b}}{(1/T_l+1/T_s)T_b}\right)\right]. \tag{15}$$

Also for C_{IO}, we find a very good agreement with the results of the Langevin equation integration.

B. Residence time distributions: averaged BER

In order to evaluate B_A we cannot use the probability densities $n_{\pm}^{0,1}$, since an ensemble average over the whole sequence would be implied. In fact, this indicator requires a specific operation within each bit which cannot be performed on the average distributions $n_{\pm}^{0,1}$. It is therefore not trivial to find an analytical expression for B_A starting from the master equation. Here we will introduce an alternative method, based on a statistical analysis of the state jumps within the single bit. We still assume that our system is described by a two-level approximation, in which the residence time distributions in a given state + or − are given by the (3).

Assuming, e.g., that the input bit is 1, we can calculate the probability density $P_{+}^{1}(T)$ to remain, on the whole, a time between T and $T+dT$ in the + state during T_b. We have to sum over all possible ways of dividing an interval of duration T_b into subintervals, having a total time of residence

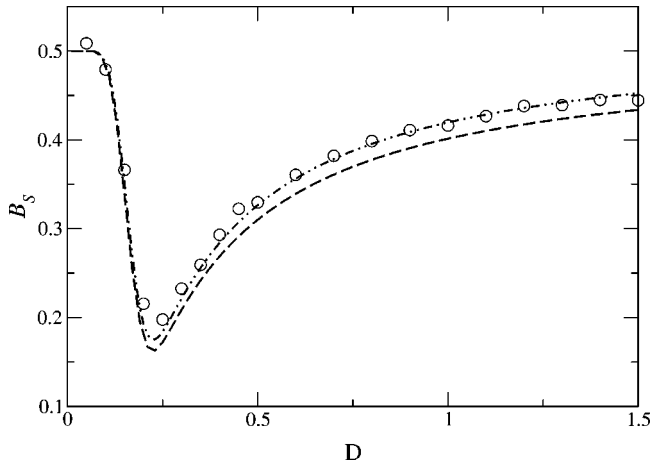

FIG. 7. Numerical and analytical calculation of the sampled BER (B_S) for the parameters given in Sec. III. B_S is obtained from the Langevin equation [Eq. (2)] integration (circles). In the analytical expression [Eq. (11)], the Kramers times are calculated using Eq. (12) (dashed line) or Eq. (13) (dot-dashed line).

in the + state equal to T. The probability of each subinterval is given by Eq. (3). We obtain

$$P_+^1(T)=\frac{1}{2}\left\{\exp\left(-\frac{T}{T_+^1}\right)\exp\left(-\frac{T_b-T}{T_-^1}\right)\times\left[\frac{T_b}{T_+^1T_-^1}\sum_{n=0}^{\infty}\frac{1}{n!(n+1)!}\left(\frac{T(T_b-T)}{T_+^1T_-^1}\right)^n+\left(\frac{1}{T_+^1}+\frac{1}{T_-^1}\right)\sum_{n=0}^{\infty}\frac{1}{(n!)^2}\left(\frac{T(T_b-T)}{T_+^1T_-^1}\right)^n\right]+\delta(T-T_b)\exp\left(-\frac{T_b}{T_+^1}\right)+\delta(T)\exp\left(-\frac{T_b}{T_-^1}\right)\right\}. \tag{16}$$

The first (second) term in square brackets comes from all the events in which the interval T_b is divided into an odd, namely, $2n+3$ (even, namely $2n$), number of subintervals. The delta terms are the contributions for the case of no jumps occurring during the bit interval [23]. The factor $\frac{1}{2}$ comes from the average over the two possible states of the system at the beginning of the bit. Equation (16) can be further reduced by summing the power series, obtaining

$$P_+^1(T)=\frac{1}{2}\left\{\exp\left(-\frac{T}{T_+^1}\right)\exp\left(-\frac{T_b-T}{T_-^1}\right)\times\left[\frac{T_b}{T_+^1T_-^1}\sqrt{\frac{T_+^1T_-^1}{T(T_b-T)}}\times I_1\left(2\sqrt{\frac{T(T_b-T)}{T_+^1T_-^1}}\right)+\left(\frac{1}{T_+^1}+\frac{1}{T_-^1}\right)\times I_0\left(2\sqrt{\frac{T(T_b-T)}{T_+^1T_-^1}}\right)\right]+\delta(T-T_b)\exp\left(-\frac{T_b}{T_+^1}\right)+\delta(T)\exp\left(-\frac{T_b}{T_-^1}\right)\right\}, \tag{17}$$

where the functions I_n are the modified Bessel functions of order n.

Similar relations hold for $P_-^0(T)$. Moreover, we have the relations:

$$P_+^{0,1}(T)=P_-^{0,1}(T_b-T). \tag{18}$$

B_A is just the probability to remain in the + state for a time longer than $T_b/2$ while the input bit is 0, or to remain in the ''-'' state while the input bit is 1, i.e.,

$$B_A=\tfrac{1}{2}\int_{T_b/2}^{T_b}[P_+^0(T)+P_-^1(T)]dT. \tag{19}$$

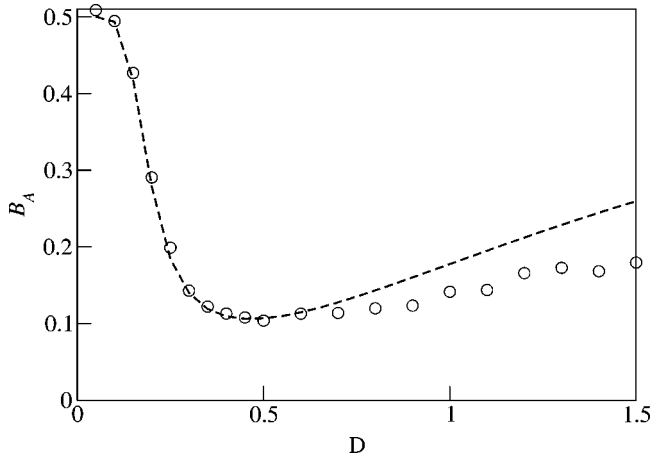

FIG. 8. Numerical and analytical calculations of the averaged BER (B_A) for the parameters given in Sec. III. B_A is obtained from an integration of the Langevin equation [Eq. (2)] (circles). In the analytical formula [Eqs. (20) and (17)], the Kramers times are calculated using Eq. (13) (dashed line).

In addition, in the symmetric case we have $P_+^1(T)=P_-^0(T)=P_l(T)$ and $P_-^1(T)=P_+^0(T)=P_s(T)$. Combining these results, one obtains

$$B_A=\int_{T_b/2}^{T_b}P_s(T)dT=\int_0^{T_b/2}P_l(T)dT. \tag{20}$$

The analytical expressions (19) and (20) are integrated numerically.

In Fig. 8 we plot the values obtained from the integration of the Langevin equation [Eq. (2)] (circles) together with the result of Eqs. (20), (17), and (13). The agreement is good as long as the noise remains smaller than the potential depth. For high noise (after the resonance) the Kramers expression for the permanence times is no longer reliable, since the time-scale separation hypothesis is no longer verified (see Refs. [17,24]). However, we stress that the comparison with the experimental results is based on an analytical calculation with experimentally measured permanence times. In this case the agreement is still good, as shown in Sec. IV.

The analytical result shown in Fig. 8 refers to specific values of A and T_b, and considers a simple potential giving a specific relation between T_l and T_s. However, the analytical expressions found for B_A are more general, and it is interesting to analyze their behavior for arbitrary values of the parameters. In Fig. 9 we report a contour plot of B_A versus the rescaled residence times T_l/T_b and T_s/T_b. The only assumption for this graph is the exponential decrease of Eq. (3) in the two states. The region above the equal times line [labeled by $-\log_{10}(2)$] is meaningless, since it would imply $T_l<T_s$. Once given T_l and T_s as functions of the noise, on the contour plot we can trace a path which gives B_A. As an example, assuming a Kramers relation for T_l and T_s [e.g., Eq. (12)], we obtain a straight path (dashed line) given by $y=ax+b$, where $a=1-2A/(\Delta V+A)$, $b=2A\log(\pi/2\sqrt{2}T_b)/(\Delta V+A)$, and (x,y) are the coordinates in the contour plot. Increasing the noise, the path is followed

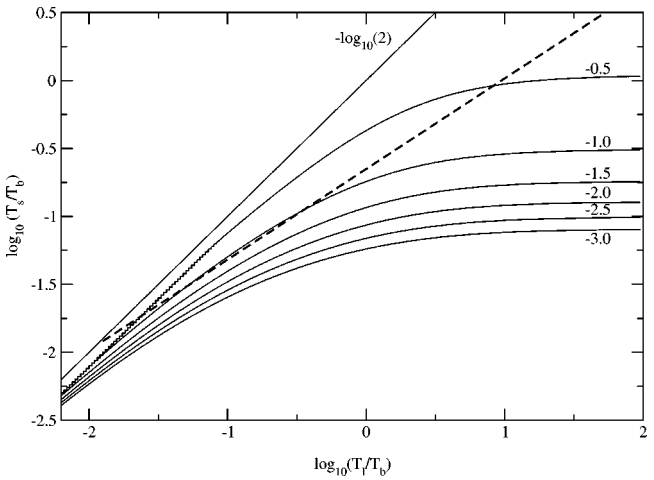

FIG. 9. Bit-averaged BER from Eq. (20) as a function of $T_{l,s}/T_b$. We plot the contour lines of $\log_{10}(B_A)$ (solid lines). The contour line $-\log_{10}(2)$ corresponds to the limiting case of a completely uncorrelated output binary signal, when $T_s=T_l$. The dashed line represents a scan on D, increasing from right to left, for the same parameters of Fig. 8. The region beyond the contour line $-\log_{10}(2)$ is meaningless, as it corresponds to $T_s>T_l$.

from the top right to the bottom left. The resonant behavior of B_A is clearly visible. The change of parameters yields a change of the slope and a shift of the path, and therefore induces a change of the resonance position and depth. Figure 9 gives a comprehensive picture of B_A behavior, for a very general system.

An inportant feature that can be inferred from Fig. 9 concerns the transmission rate. As the meaningful physical quantities are the rescaled residence times, the bit duration T_b can be arbitrarly reduced, providing that a suitable amount of noise accordingly reduces the Kramers times. Of course, in a real system the transmission rate is limited by effects which are not included in our simple description. Some examples in our system are the finite jump time between the two polarizations (about 10 ns); the noise introduced in the laser current, which also produces fluctuations in the total intensity, which eventually mask the signal; and the quasipotential, that does not follow istantaneously the modulation on the pump current. This last point is presently subject of investigations. Using the probability densities, the correlation C_{IO} can also be evaluated as

$$C_{IO}=\tfrac{1}{2}\int_0^{T_b} dT\,\frac{2T-T_b}{T_b}[P_+^1(T)+P_-^0(T)], \qquad (21)$$

obtaining the same result as in Sec. II.

IV. DISCUSSION

In this section we compare the numerical and analytical results with the experimental measurements, and discuss the physical contents of the phenomena. In Ref. [13] we already reported a preliminary investigation of the system behavior, based on the study of the correlation C_{IO}. For the sake of completeness, here we summarize the main points. In Fig. 2, we compare the experimental data with the prediction of Eq. (14), where the typical times $T_{\pm}^{0,1}$ are measured as described in Sec. II.

The agreement is very good. However, in order to shade light on the underlying physical processes, we consider the limiting cases of low and high noise. Indeed, the resonance results from two independent processes, whose effects on the output signal reproduction are monotonic with noise and opposite.

For low noise, the system response during each bit is strongly influenced by the final output state in the previous bit. For high noise, fast fluctuations are found in the response [see Figs. 1(d) and 1(e)], again leading to a decorrelation of the output signal versus the input. The ratio T_l/T_s decreases toward unity, and C_{IO} vanishes.

A simple estimation of the input-output correlation C_{IO} can be given in these two limiting cases. For low noise, we consider that at most one single jump toward the right output state can occur within a bit: this first jump is necessary to lose the memory of the previous state. This amounts to saying that $T_l\to\infty$. When the system is in the wrong state at the beginning of the bit interval, in order to induce a state flip, the residence time in the wrong state (T_s) must be shorter enough than the bit length. The correlation can be evaluated as the sum of two contributions, corresponding to the system starting, respectively, in the right state (and remaining there) and in the wrong state (with one jump to the right one within the bit):

$$C_{IO}\simeq\frac{1}{2}+\frac{1}{2}\left\{\int_0^{T_b}\frac{T_b-2t}{T_bT_s}\exp\left(-\frac{t}{T_s}\right)dt-\exp\left(-\frac{T_b}{T_s}\right)\right\}$$
$$=\frac{T_s}{T_b}\left[\exp\left(-\frac{T_b}{T_s}\right)-1\right]+1. \qquad (22)$$

For high noise, many jumps occur within a bit; thus $C_{IO}\simeq N(T_l-T_s)/T_b$, where $N=T_b/(T_l+T_s)$ is the (average) number of jumps, giving

$$C_{IO}\simeq\frac{T_l-T_s}{T_l+T_s}. \qquad (23)$$

The plots of Eqs. (22) and (23), evaluated using the experimental residence times, are reported in Fig. 10, showing a very good agreement with the experimental data. In Fig. 4 the experimental measurements of B_A are compared with the analytical expression [Eq. (19)]. The Kramers times $T_{\pm}^{0,1}$ are measured as described in Sec. II. The agreement is excellent, above all for a noise higher than 200 mV_{RMS}. Below this value, the uncertainty in the evaluations of the Kramers times leads to a poor accuracy of the theoretical predictions. The same considerations can be formulated for B_S (see Fig. 3), where the mentioned effect at low noise is more evident. However, the overall agreement is still very good.

Both correlations C_{IO} and B_A quantify the distance between input and output signals within a bit duration. While C_{IO} uses a continuous range of values, a threshold-based decision is used for B_A. The result is then averaged over the

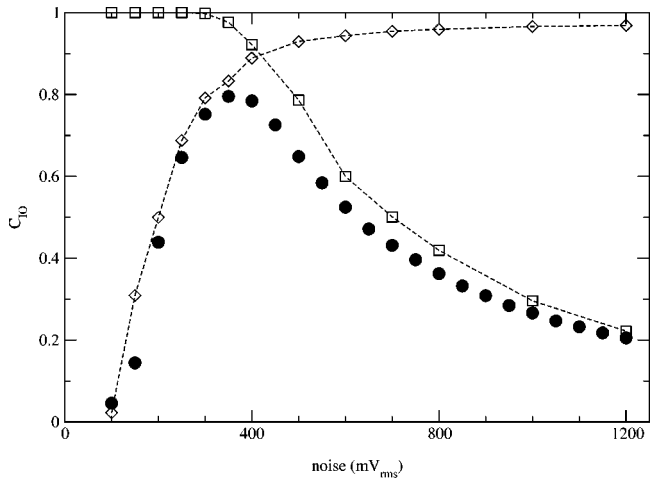

FIG. 10. Normalized input-output cross correlation. Dots: experimental data. The asymptotic results for low noise [Eq. (22), diamonds] and high noise [Eq. (23), squares] are shown using the experimental Kramers rates for the calculations. The dashed lines are guides for the eye.

whole bit sequence. To draw a link between these two indicators, let us consider the random variable d_{IO}, defined on a given input bit as

$$d_{IO}=\frac{1}{T_b}\int_0^{T_b} dt[x_{in}(t)-\overline{x_{in}}][x_{out}(t)-\overline{x_{out}}]. \qquad (24)$$

d_{IO} measures the cross-correlation on a given input bit between input and output. It is positive if the output bit is ''right'' (i.e., matches the input one), and negative otherwise. It is easy to see that the correlation C_{IO} is the average of d_{IO} over the ensemble of input bits, while B_A is the area of the normalized distribution $Q(d_{IO})$ between $-\infty$ and zero.

In Fig. 11 we show the shapes of $Q(d_{IO})$ for low noise (a), before resonance (b), close to resonance (c), and for high noise (d), obtained from the experimental data. For a low noise level, the distribution $Q(d_{IO})$ shows two sharp peaks of nearly equal intensities almost, symmetric around 0. The correlation is then very small, since the two peaks average to 0, while B_A is found close to 1/2. As the noise increases, the peaks corresponding to the wrong output bits decreases to the benefit of the other one, and the two peaks broaden. Close to resonance, the left peak almost merges with the right one, indicating that the system follows the input sequence rather well. The distribution is very asymmetric, leading to a strong cross-correlation, and the probability for d_{IO} to be negative is very small, resulting in a small B_A. For high noise, the distribution tends toward a Gaussian, as one expects from the complete randomization of the system. Its center tends slowly toward 0 as the noise increases, explaining the slow decrease (increase) of the cross-correlation (B_A) versus noise.

The discussion of B_S behavior is even simpler, and in this case the resonance is also the result of two independent phenomena. For low noise, one bit length is not enough to loose memory of the previous bit state. As the noise is increased and the residence times shorten, this effect becomes less important. With the usual approximation $T_l \gg T_b$ the expression for B_S for low noise is

$$B_S \simeq \frac{1}{2}\exp\left(-\frac{T_b}{T_s}\right). \qquad (25)$$

For high noise, when the memory effect is negligible, the probability to obtain the right bit value approaches $T_s/(T_s+T_l)$. According to the Kramers law [17], this expression decreases with noise. With respect to the other two indicators, a shorter time is sufficient to get rid of the memory effect (giving a steeper decrease of the BER), while for high noise B_S is higher than B_A.

A significant difference between classical SR and the phenomenon presented here concerns the possibility of interpreting the resonance as a time-scale matching. The statistical synchronization in SR is obtained when the average time

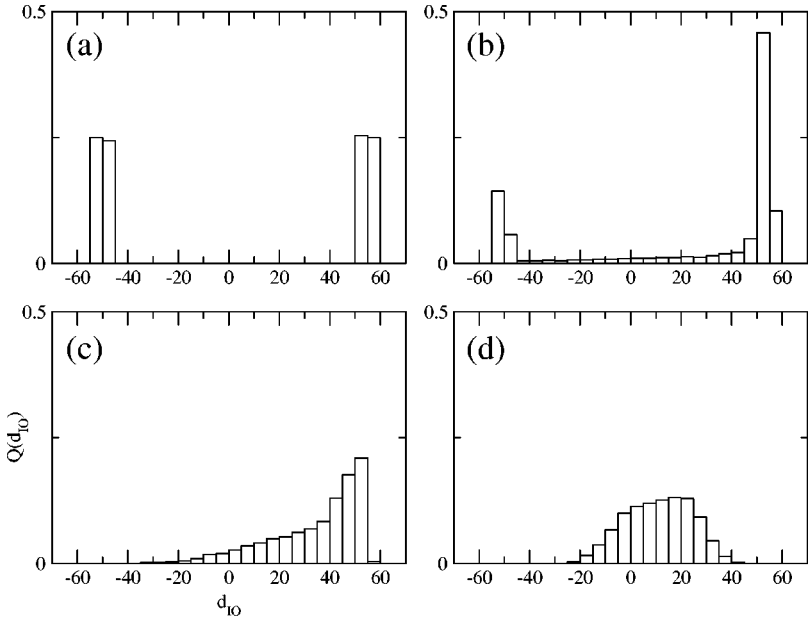

FIG. 11. Plot of the normalized distribution $Q(d_{IO})$ [see Eq. (24)] for different input noises: from left to right and top to bottom, 100, 200, 500, and 1200 mV_{rms}. The horizontal axis is in arbitrary units.

$T_K(D)$ between two successive noise-induced transitions is comparable with half the modulation period T_Ω. Therefore, the approximate SR matching condition reads

$$2T_K(D) \simeq T_\Omega . \tag{26}$$

In our system, an equivalent condition in fact does not hold. The characteristic time scale of the input signal is now T_b. As we discussed, this period must be compared with T_s and T_l: a few T_s are necessary in order to lose the memory of the previous bit; on the other hand, T_l must be long with respect to T_b:

$$\begin{aligned} T_s &\ll T_b , \\ T_l &\gg T_b . \end{aligned} \tag{27}$$

In other words, the two conditions (27) define a region for D where the output well reproduces the input signal. Even if an optimal value of D is found, it cannot be considered as a real resonance (or a time-scale matching), but rather as the best compromise naturally arising between the two requirements. Such an optimal value depends on the choice of the indicator. Moreover, both T_s and T_l depend on both the input noise and the signal amplitude A. A higher value of A yields a larger ratio T_l/T_s and therefore a wide region of D where the input signal is well reproduced, in addition to a better value of the indicators.

V. CONCLUSIONS

We have presented an experimental and theoretical analysis of noise-assisted transmission of binary information through a bistable optical system. The phenomenon is a particular example of aperiodic stochastic resonance, and in this work the predictions of theoretical models are compared with sufficiently accurate experimental findings. The phenomenon is first analyzed by considering the complete time evolution of the bistable system, by means of the input-output correlation. Moreover, we have studied the binary information flow by using appropriate indicators. Both analytical expressions and numerical simulations are in quantitative agreement with the measured quantities. The analysis of the low- and high-noise limit cases leads to a clear picture of the phenomenon, showing that the ''resonance'' is more precisely described as a crossing region of two independent processes, whose effects on the output signal reproduction are monotonic with noise and opposite.

ACKNOWLEDGMENTS

This work was partially supported by EU network HPRN-CT-2000-00034 ''VCSEL's for Information Society Technology Applications'' (VISTA). S. B. acknowledges EU support through the TMR Grant ''Marie-Curie'' No. ERBFMBICT983351.

[1] R. Benzi, A. Sutera, and A. Vulpiani, J. Phys. A **14**, 453 (1981); R. Benzi, G. Parisi, A. Sutera, and A. Vulpiani, Tellus **34**, 10 (1982).
[2] C. Nicolis and G. Nicolis, Tellus **33**, 225 (1981).
[3] B. McNamara, K. Wiesenfeld, and R. Roy, Phys. Rev. Lett. **60**, 2626 (1988).
[4] See, e.g., L. Gammaitoni, P. Hänggi, P. Jung, and F. Marchesoni, Rev. Mod. Phys. **70**, 223 (1998), and references therein.
[5] G. Giacomelli, F. Marin, and I. Rabbiosi, Phys. Rev. Lett. **82**, 675 (1999).
[6] S. Barbay, G. Giacomelli, and F. Marin, Phys. Rev. E **61**, 157 (2000).
[7] A. Neiman and L. Schimansky-Geier, Phys. Rev. Lett. **72**, 2988 (1994).
[8] J.J. Collins, C.C. Chow, and T.T. Imhoff, Phys. Rev. E **52**, R3321 (1995); Nature (London) **376**, 236 (1995).
[9] J.J. Collins, C.C. Chow, A.C. Capela, and T.T. Imhoff, Phys. Rev. E **54**, 5575 (1996).
[10] A. Neiman, L. Schimansky-Geier, F. Moss, B. Shulgin, and J.J. Collins, Phys. Rev. E **60**, 284 (1999).
[11] F. Chapeau-Blondeau, Phys. Rev. E **55**, 2016 (1997).
[12] P. Cordo *et al.*, Nature (London) **383**, 769 (1996); J.J. Collins, T.T. Imhoff, and P. Grigg, *ibid.* **383**, 770 (1996); J. Neurophysiol. **76**, 642 (1996); E. Simonotto *et al.*, Phys. Rev. Lett. **78**, 1186 (1997); A. Fulinski, Chaos **8**, 549 (1998), and references therein.
[13] S. Barbay, G. Giacomelli, and F. Marin, Phys. Rev. Lett. **85**, 4652 (2000).
[14] S. Barbay, G. Giacomelli, and F. Marin, Opt. Lett. **25**, 1095 (2000); Un procedimento ed un dispositivo di trasmissione ottica di informazioni codificate, Italian patent, February 15, 2000.
[15] J. van't Hoff, in *Etudes de Dynamiques Chimiques* (Muller, Amsterdam, 1884).
[16] S. Arrhenius, Z. Phys. Chem. (Leipzig) **4**, 226 (1889).
[17] H. Kramers, Physica (Utrecht) **7**, 284 (1940).
[18] M. San Miguel, Q. Feng, and J.V. Moloney, Phys. Rev. A **52**, 1728 (1995); J. Martin-Regalado, F. Prati, M. San Miguel, and N.B. Abra-ham, IEEE J. Quantum Electron. **33**, 765 (1997).
[19] M.B. Willemsen, M.U.F. Khalid, M.P. van Exter, and J.P. Woerdman, Phys. Rev. Lett. **82**, 4815 (1999).
[20] J. Danckaert, B. Nagler, J. Albert, K. Panajotov, I. Veretennicoff, and T. Erneux (unpublished).
[21] G. Giacomelli and F. Marin, Quantum Semiclassic. Opt. **10**, 469 (1998).
[22] R.L. Honeycutt, Phys. Rev. A **45**, 600 (1992).
[23] We assume that $\int_a^b \delta(x-x_0) f(x) dx = f(x_0)$ if $x_0 \in [a,b]$ (extrema included).
[24] P. Hänggi, P. Talkner, and M. Borkovec, Rev. Mod. Phys. **62**, 251 (1990).